Applied Catalysis B: Environmental 304 (2022) 121010

Contents lists available at ScienceDirect

Applied Catalysis B: Environmental

journal homepage: www.elsevier.com/locate/apcatb

Surface synergetic effects of Pt clusters/monolayer Bi_2MoO_6 nanosheet for promoting the photocatalytic selective reduction of 4-nitrostyrene to 4-vinylaniline

Yingzhang Shi, Zhiwen Wang, Cheng Liu, Tai kang Wu, Rui Liu, Ling Wu *

State Key Laboratory of Photocatalysis on Energy and Environment, Fuzhou University, Fujian 350116, Fuzhou, China

ARTICLE INFO

Keywords:
Pt clusters
Monolayer Bi_2MoO_6 nanosheet
Selective reduction of 4-nitrostyrene
Photocatalytic hydrogen transfer
Coordination activation

ABSTRACT

Pt clusters supported on monolayer Bi_2MoO_6 nanosheets (Pt/BMO-NS) are constructed for the photocatalytic selective reduction of 4-nitrostyrene to 4-vinylaniline in the presence of $HCOONH_4$ and exhibit high conversion (≈100%) of 4-nitrostyrene and high selectivity (≈100%) of 4-vinylaniline. *In situ* FTIR spectra and XPS spectra of BMO-NS absorbed 4-nitrostyrene further demonstrate that 4-nitrostyrene can be selectively absorbed and activated on surface Mo^{5+} and Bi^{2+} sites of BMO-NS via the Bi···O-N or Mo···O-N coordination. The Pt clusters and photogenerated carriers synergistically make the efficient dissociation of $HCOO^-$ to form rich $\cdot CO_2^-$ and active ·H, greatly supporting the selective reduction of 4-nitrostyrene to 4-vinyaniline. This work not only highlights the complete utilization of photo-generated carriers to achieve the selective reduction of 4-nitrostyrene to 4-vinylaniline via photocatalytic hydrogen transfer, but also uses metal/monolayer nanosheets as a molecule platform to deeply study the surface/interface synergetic mechanism at the molecule level.

1. Introduction

Aromatic amines and their derivatives, especially with other reducible groups, are very useful intermediates for the productions of dyes, agrochemicals, polymers and pharmaceuticals [1–3]. Generally, the synthesis of aromatic amines is to reduce their corresponding nitro compounds [4,5]. The selective reduction of nitro group when other reducible organic groups such as alkynes, alkene, aldehydes, halogen, ketones and nitriles are present is still a very difficult but significant task [6]. 4-vinylaniline as a high valued organic intermediate is a representative aromatic amine that can be produced by the selective reduction of 4-nitrostyrene [7,8]. The key issue for the selective reduction of 4-nitrostyrene to 4-vinylaniline is to selectively absorb and reduce the $-NO_2$ group while the sensitive -C═C group is present. However, traditional thermal catalysis is hard to address this problem due to the -C═C group being unstable in a high temperature and high-pressure environment [9,10]. It is necessary to develop a new mild route to achieve the selective reduction of 4-nitrostyrene to 4-vinylaniline. In recent years, a new photocatalytic route for organic transformation may be potential to address this due to its mild, environmentally friendly and controllable advantages [11–16]. However, low photocatalytic efficiency and unclear surface/interface catalytic mechanism still limit its development. Therefore, it is a meaningful challenge for us to design an appropriate photocatalyst that would achieve the efficient selective reduction of 4-nitrostyrene to 4-vinylaniline and provide deep insight for understanding the surface/interface interaction between the 4-nitrostyrene molecules and the active sites.

To achieve the precise synthesis of 4-vinylaniline from 4-nitrostyrene, one of the important factors that need to be considered is the hydrogen source. Traditional thermal catalysis uses H_2 as hydrogen source for selective hydrogenation of 4-nitrostyrene to 4-vinylaniline with additional temperature and pressure [17]. Moreover, the metal hydrides like $NaBH_4$ or $LiAlH_4$ as reducing agents and hydrogen source are also used for hydrogenation reactions [18,19]. However, using the explosive and flammable high pressure H_2 and expensive metal hydrides to reduce 4-nitrostyrene is unworthy and the selectivity of 4-vinylanailine is hard to control. Catalytic hydrogen transfer which uses small organic molecules like formic acid or its salts, oxalic acid or its salts, alcohols and other organic molecules as hydrogen source is promising alternatives of H_2 for hydrogenation reactions because these small molecules are safer, lower cost and more controllable [20–22]. Ammonium formate is a very representative small molecule hydrogen source for the reduction of the nitro compounds. It has been reported that the photo-generated holes of a photocatalyst can dissociate ammonium

* Corresponding author.
E-mail address: wuling@fzu.edu.cn (L. Wu).

https://doi.org/10.1016/j.apcatb.2021.121010
Received 12 October 2021; Received in revised form 6 December 2021; Accepted 8 December 2021
Available online 10 December 2021

formate to $\cdot CO_2^-$ and H^+, serving as reductive species and hydrogen source for the reduction of nitro group, respectively [23]. The $\cdot CO_2^-$ with strong reducing ability facilitates the preferential reduction of electron-deficient -NO_2 group, promoting the conversion of 4-nitrostyrene towards 4-vinylaniline. Therefore, a photocatalyst with the ability for efficiently dissociating ammonium formate may be a good candidate for the selective reduction of 4-nitrostyrene to 4-vinylaniline when using ammonium formate as hydrogen source.

Another very effective strategy to achieve the precise synthesis of 4-vinylaniline is to design specific sites for the photocatalysts to selectively absorb and activate -NO_2 groups. It requires us to understand the adsorption behavior of 4-nitrostyrene over a photocatalyst because that the adsorption modes and adsorption strength of -C═C and -NO_2 groups would greatly influence the selectively of 4-vinylaniline in a large extent. The -C═C group is an electron-rich group which can be absorbed on the electrophilic sites, achieving the selective hydrogenation of the -C═C group [6]. Quite the opposite, the -NO_2 group is an electron-deficient group which trends to be absorbed on the nucleophilic sites of the catalysts [24]. Meanwhile, these nucleophilic sites would also repel the electron-rich -C═C group. This absorption mode avails the selective reduction of 4-nitrostyrene to 4-vinylaniline. Thus, designing a photocatalyst with rich nucleophilic sites, such as Lewis base sites, maybe hopeful to selective absorb and activate the -NO_2 group, achieving the precise conversion of 4-nitrostyrene to 4-vinylaniline.

Bi_2MoO_6 with a typical Aurivillius layer structure, which consists of the alternating layer between $[MoO_4]^{2-}$ and $[Bi_2O_2]^{2+}$, has exhibited impressive photocatalytic performance for the CO_2 reduction, organic pollutant degradation and selective organic transformation due to its suitable energy band positions [25–28]. Some previous studies also reported that Bi_2MoO_6 can reduce nitrobenzene to aniline, confirming the feasibility for reducing -NO_2 group over Bi_2MoO_6 [29]. However, there are few studies devote to reveal the main active sites of Bi_2MoO_6 and deeply study the surface/interface interaction between the reactants and the active sites. Nowadays, two-dimensional (2D) materials, especially with only monolayer or several atomic layer thicknesses, have obtained extensive attention because of their prominent merits such as ultrathin nanosheets nature, larger specific surface area, abundant surface unsaturated sites and better ability for photogenerated carrier separation [30–34]. Meanwhile, 2D nanosheet is an ideal platform to investigate the surface/interface interaction between the reactants and a photocatalyst. In view of this, our group has developed a series of nanosheets for photocatalytic organic synthesis, such as HNb_3O_8 [35], Bi_2MoO_6 [36], BiOCl and ZnTi-LDH [37]. It is revealed that ultrathin nanosheets would expose rich surface Lewis acid/base sites to selective absorb specific organic groups, achieving the precise transformation from reactant to target product. In addition, ultrathin nanosheet structure benefits to support the evenly dispersed metal nanoparticles as co-catalyst to further enhance the photocatalytic performance via the synergistic effects between metals nanoparticles and ultrathin nanosheets [38]. The loading of metal nanoparticles not only makes the surface functionalization of nanosheets but also promotes the efficient separation of photo-generated carriers via metal−support interface effects [39]. Our latest work has revealed that Pt nanoclusters can decompose ammonium formate to produce $\cdot CO_2^-$ and active ·H for reducing nitrobenzene [40]. Thus, based on the above idea, monolayer Bi_2MoO_6 nanosheets with evenly dispersed Pt nanoparticles can be properly designed to achieve the selective reduction of 4-nitrostyrene to 4-vinylaniline and serve as a molecular platform to investigate the surface/interface interaction between the reactants and the active sites.

Herein, Pt clusters decorated monolayer Bi_2MoO_6 nanosheets are successfully constructed for the selective reduction of 4-nitrostyrene to 4-vinylaniline under visible light irradiation using ammonium formate as a hydrogen source. The prepared samples are well studied by XRD, SEM, TEM, AFM, XPS to reveal their phase structure, morphology and surface chemical states. A series of controlled experiments are conducted to investigate the influence of Pt, BMO-NS, temperature, hydrogen source and time for the selective reduction of 4-nitrostyrene to 4-vinylaniline. The surface Lewis base sites of prepared monolayer Bi_2MoO_6 nanosheets are revealed by CO_2-TPD test. In addition, in situ FTIR spectra and XPS spectra of BMO-NS absorbed 4-nitrostyrene are used to deeply ascertain the surface/interface interaction of 4-nitrostyrene molecule over BMO-NS. The active species of $\cdot CO_2^-$ are also confirmed using EPR technique. Based on the above results, we proposed a possible photocatalytic mechanism for the selective reduction of 4-nitrostyrene to 4-vinylaniline over Pt/BMO-NS at a molecular level.

2. Experimental section

2.1. Synthesis for monolayer Bi_2MoO_6 nanosheets (BMO-NS) and bulk Bi_2MoO_6 (BMO-bulk)

The BMO-NS was synthesized via a typical hydrothermal method using cetyltrimethylammonium bromide (CTAB) as a surfactant [29]. 1 mmol $Na_2MoO_4.2H_2O$ and 0.05 g of CTAB were dissolved in 80 mL of deionized water with vigorous stirring. 2 mmol $Bi(NO_3)_3.5H_2O$ were added into the above mixture for 1 h stirring. Then, the mixture was transferred into a 100 mL Teflon-lined autoclave and was put in an oven at 100 ℃ for 24 h. After the reaction, the solid products were washed with deionized and ethanol to remove the excess ions. Finally, the yellow solid samples were dried in a vacuum oven at 60 ℃ for 12 h. The BMO-bulk sample was prepared by the same procedure without adding CTAB.

2.2. Synthesis for Pt clusters/monolayer Bi_2MoO_6 nanosheets (Pt/BMO-NS)

A photo-deposition method was used to prepare 1 wt% of Pt/BMO-NS. The prepared BMO-NS was dispersed in 50 mL of deionized water under vigorous stirring. The solution of $H_2PtCl_6.6H_2O$ (10 mg/mL) was dripped slowly into the colloidal solution of BMO-NS. Then, 5 mL of methanol as a hole sacrificial agent was added to the mixture. The mixture was stirred in N_2 atmosphere to remove O_2 and was irradiated under a 300 W Xenon lamp (Beijing Perfect Light Co. Ltd., PLS-SXE300D.) for 2 h. The final product was washed with ethanol and deionized water and collected by centrifugation and dried at 60 ℃ for 12 h. In addition, Pt/ BMO -bulk was prepared via the same procedure. The actual mass content of Pt is measured by ICP-OES (inductively coupled plasma optical emission spectrometry, Table S3), which is close to the calculated value.

2.3. Characterization

An Ultima IV X-ray diffractometer with Cu-Kα radiation (λ = 1.5418 Å) was used to record the X-ray diffraction (XRD) patterns of the prepared samples in the range 5–60°. Scanning electron microscope (SEM) images of all the samples were obtained using an FEI Quanta 200 F electron microscope. Transmission electron microscopy (TEM), element mapping and higher-resolution transmission electron microscopy (HRTEM) were performed using a JEOL model JEM2010 EX microscope. A Bruker Dimension Icon was used to test the atomic force microscopy (AFM) image of the sample. Ultraviolet- visible diffuse reflectance spectra (UV–vis DRS) of the prepared samples were measured on a UV–vis spectrophotometer (Cary 500). X-ray photoelectron spectroscopy (XPS) spectra were obtained on a PHI Quantum 2000 XPS system with monochromatic Al Kα Radiation. The electrochemical impedance spectroscopy, photocurrent measurements and Mott-Schottky plots were respectively conducted on the Zahner electrochemical workstation and a CHI660D electrochemical workstation. N_2 adsorption-desorption results were obtained on a Micrometrics ASAP 2020 M. Electron paramagnetic resonance (EPR) spectra of the prepared samples were recorded using a Bruker EPR A300 spectrometer. Inductively coupled plasma optical emission spectrometry (ICP-OES) was obtained on PerkinElmer (Avio

200).

2.4. In situ FTIR measurement

The in situ FTIR spectra of 4-nitrostyrene absorbed over the photocatalysts were recorded on a Nicolet Nexus 670 Fourier transform infrared (FT-IR) spectrometer with a resolution of 4 cm^{-1} for 64 scans. Firstly, 20 mg of the photocatalysts were pressed into a wafer and anchored into a self-supporting IR disk. Then, this disk was put into a samples holder with a cell's tube. To remove the contaminants over the surface of the photocatalyst, the photocatalyst was treated at 180 ℃ for 3 h under a dynamic vacuum (5×10^{-4} Torr). The FTIR spectrum of the initial photocatalyst was recorded. Then 10 μL of 4-nitrostyrene was added to the photocatalyst using a syringe. After 20 min, the next FTIR spectrum of the photocatalyst with 4-nitrostyrene was collected. The sample was further treated at 150 ℃ for 5 min under a dynamic vacuum (5×10^{-4} Torr). After this process, the final FTIR spectrum was collected.

2.5. Photocatalytic reduction of 4-nitrostyrene to 4-vinylaniline

The reduction of 4-nitrostyrene was conducted in an oxygen-free reaction tube. 10 mg of the catalyst, 0.1 mmol of 4-nitrostyrene and 1.5 mL of $HCOONH_4$/methanol saturated solution were added to the reaction tube. The Ar was used to flush the mixture for removing O_2. After 10 min, the reaction tube was irradiated using a 300 W Xenon lamp (Beijing Perfect Light Co. Ltd., PLS-SXE300D.) with a 400 nm cut-off filter. The photocatalytic reaction is conducted under stir to make the photocatalyst evenly dispersed in the solution. After irradiation for 4 h, the mixture was centrifuged to remove the solid catalyst. The resultant solution was analyzed using a Shimadzu Gas Chromatograph (GC2014C) which was equipped with a hydrogen flame ionization detector (FID) and a Shimadzu SH-RTX-S column (30 m * 0.25 μm * 0.32 mm). The conversion of 4-nitrostyrene and the selectivity for 4-vinylaniline were calculated using the following equations:

$$\text{Conversion } (\%) = [(C_0 - C_{4\text{-nitrostyrene}})/C_0] \times 100\%$$

$$\text{Selectivity } (\%) = [C_{4\text{-vinylaniline}}/(C_0 - C_{4\text{-nitrostyrene}})] \times 100\%$$

The initial and final concentration of 4-nitrostyrene is denoted as C_0 and $C_{4\text{-nitrostyrene}}$, and the concentration of 4-vinylaniline is denoted as $C_{4\text{-vinylaniline}}$. The absorption of 4-nitrostyrene over the photocatalyst is ignored.

3. Results and discussion

3.1. Characterization of the prepared samples

Fig. 1a shows the XRD patterns of the prepared samples, including BMO-Bulk, Pt/BMO-Bulk, BMO-NS and Pt/ BMO-NS. All the XRD patterns are well matched with an orthorhombic phase Bi_2MoO_6 (JCPDS No. 21–0102), indicating that the orthorhombic phase Bi_2MoO_6 are successfully synthesized [25]. It also can be clearly noted that the crystallinity of BMO-NS is lower than that of BMO-bulk, suggesting the nanostructure nature of BMO-NS. After loading Pt nanoparticle on Bi_2MoO_6, negligible changes can be observed in the XRD patterns of Pt/BMO-Bulk and Pt/ BMO-NS, suggesting that Bi_2MoO_6 samples can keep pristine crystal structure after photo-deposition. Moreover, Pt (111) diffraction peak at 39.7° is not observed in Pt/BMO-Bulk and Pt/ BMO-NS. It may be attributed to the small loading amount or this signal to be masked by the diffraction peak of Bi_2MoO_6 (240) at 39.1° [41]. TEM image of BMO-NS (Fig. 1b) exhibits transparent nanosheets, indicating that ultrathin BMO-NS nanosheet is prepared successfully. The nanosheets structure can be also observed in the SEM image of BMO-NS (Fig. 1d). Besides, the selected-area electron diffraction (SAED) image (Fig. 1c) shows a series of bright spots which are indexed to the [020] zone axis of the BMO-NS, demonstrating that BMO-NS ultrathin nanosheets have the typical single crystalline features [25]. Furthermore, AFM image is used to reveal the thickness of the BMO-NS nanosheet. As shown in Fig. 1e, the average thickness of BMO-NS is about 0.88 nm, corresponding to a unit cell thickness of the BMO (Fig. S2). This result

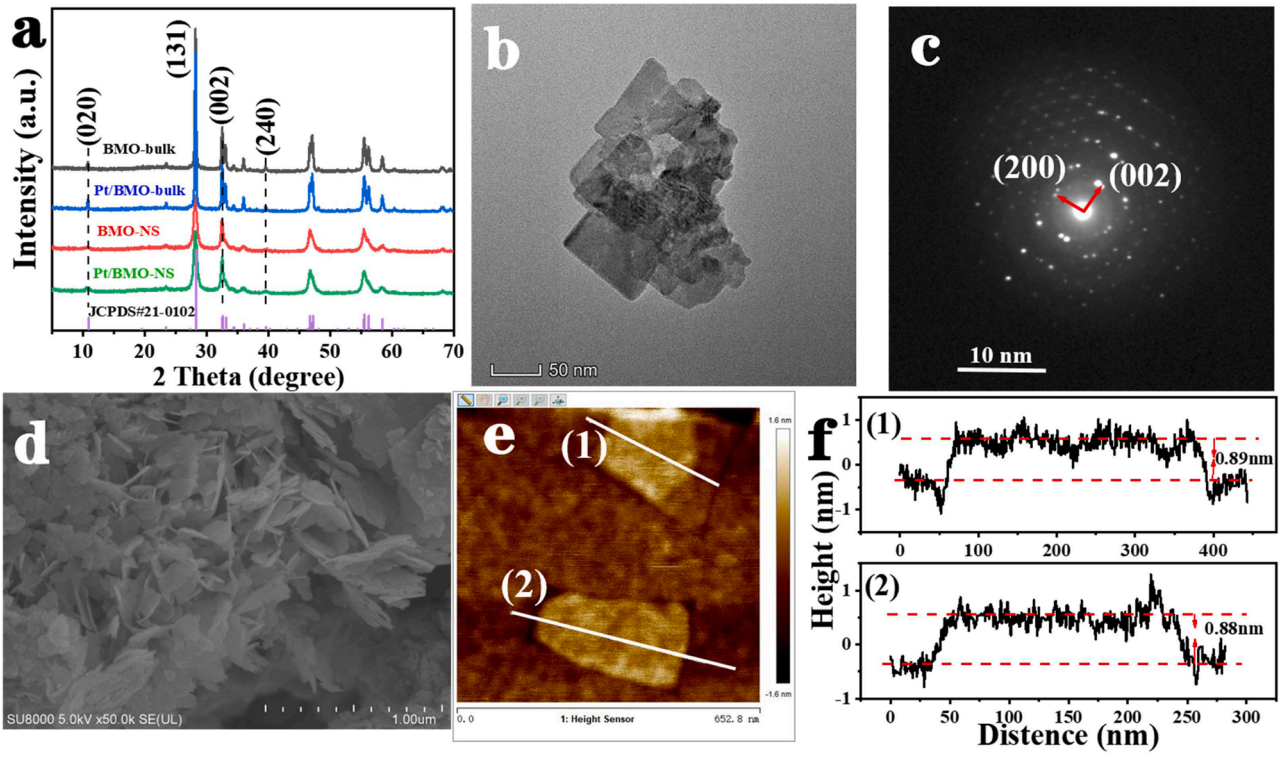

Fig. 1. XRD patterns of the prepared samples (a), TEM (b), SAED (c), SEM (d), AFM (e) images and the height profiles (f) of BMO-NS.

indicates the successful preparation of the monolayer BMO-NS nanosheet. In addition, SEM image of Pt/BMO-NS (Fig. S1b) also exhibits nanosheets structure, suggesting that BMO-NS still retains the nanosheet structure after photo-deposition. However, Pt nanoparticles can't be observed in Fig. S1b because that the Pt nanoparticle size is too small to observe.

To confirm that Pt nanoparticles are successfully loaded on BMO-NS, TEM test for Pt/BMO-NS is conducted. As shown in Fig. 2a, TEM image shows that Pt/BMO-NS are ultrathin nanosheets with evenly distributed nanoparticles while HRTEM image (Fig. 2b) exhibits clear lattice fringes with the distance of 0.227 nm which is attributed to the Pt (111) crystalline plane [42]. This confirms that the successful formation of Pt nanoparticles on the surface of BMO-NS. Moreover, the size distribution of Pt (Fig. 2c) demonstrates that the average diameter of Pt is only about 1.5 nm. These small Pt nanoparticles can be regarded as nanoclusters. Furthermore, element mapping images (Fig. 2d) also confirm the uniform distribution of Pt element over BMO-NS. Therefore, all the results suggest that the composite photocatalyst of BMO-NS with evenly dispersive Pt clusters is constructed successfully.

The surface chemical states of prepared samples are further investigated by the XPS spectra. As shown in Fig. 3a, the Bi 4*f* spectra of BMO-bulk, BMO-NS and Pt/BMO-NS exhibit two main peaks with binding energy at 164.5 eV and 159.2 eV which are respectively attributed to Bi $4f_{7/2}$ and Bi $4f_{5/2}$, revealing that the main chemical state of Bi is Bi^{3+}. Moreover, two small peaks at 163.5 eV and 158.2 eV can be observed in the XPS spectra of BMO-NS and Pt/BMO-NS, which are attributed Bi^{2+}, indicating that the Bi element in BMO-NS and Pt/BMO-NS have a higher electron cloud density than that in BMO-bulk [43]. This phenomenon also exists in Mo 3*d* spectra (Fig. 3b). The XPS spectra of Mo 3*d* have two main peaks at 235.6 eV and 232.5 eV which correspond to Mo^{6+} [25]. In addition, for the Mo 3*d* spectra of BMO-NS and Pt/BMO-NS, Mo^{5+} at bind energy 234.7 eV and 231.6 eV can be fitted [44,45]. The reason for the formation of Bi^{2+} and Mo^{5+} is that monolayer nanosheets structure would make rich surface unsaturated atoms be exposed, breaking the balance in the charge distribution [46]. It also reveals that monolayer BMO-NS have rich surface unsaturated states, especially the surface Bi^{2+} and Mo^{5+} with a higher electron cloud density, which can serve as nucleophilic sites to selective absorb -NO_2 groups. Moreover, the XPS fitting results (Table S1) also reveal the fraction of the surface elements. Especially, it can be clearly observed that the surface Bi^{2+} and Mo^{5+} proportion is increased after loading Pt clusters. The possible reason is that the photo-generated electrons would transfer to the surface of BMO-NS during the photo-deposition process, resulting in the surface charge enrichment. It would provide more nucleophilic sites for selectively absorbing -NO_2 groups in the photocatalytic process. Furthermore, O 1*s* peaks (Fig. 3c) at 530.2 eV are observed for all the samples, which are assigned to lattice oxygen [47]. The Pt 4*f* spectra as shown in Fig. 3d, the binding energy of 74.9 eV and 71.6 eV are respectively assigned to Pt $4f_{5/2}$ and Pt $4f_{7/2}$, demonstrating that the main valence state of Pt clusters in Pt/BMO-NS is metallic Pt^0. There are also two peaks at 75.9 eV and 72.6 eV, indicating a small number of Pt^{2+} is existed in Pt/BMO-NS [48]. The ratio of Pt^{2+} and Pt^0 is 19% and 81%, respectively (Table S1). The formation of Pt^{2+} may be because of the strong interfacial interaction between BMO-NS and Pt nanoclusters. It would be a bridge to connect BMO-NS and Pt clusters, which not only facilitates the transfer of the photogenerated electrons but also make the firm anchoring of Pt clusters over BMO-NS.

The UV–vis DRS spectra of the prepared samples are used to study their light absorption properties. As shown in Fig. S3, it is obvious that all the samples can absorb visible light. After loading Pt clusters, the ability of Pt/BMO-bulk and Pt/BMO-NS for absorbing visible light is promoted. The band gap width of BMO-bulk and BMO-NS (Fig. S4a) are 2.48 eV and 2.56 eV, respectively. Moreover, Mott-Schottky plot reveals that the flat-band potential of BMO-NS (Fig. S5b) is − 0.55 V vs. Ag/AgCl at pH 7, corresponding to − 0.35 V vs. NHE. Meanwhile, the positive slopes of Mott-Schottky curves suggest that BMO is an n-type semiconductor. It is reported that the flat band potential and CB potential of n-type semiconductor are approximately equal [49]. Therefore, the CB potential of BMO-NS is about − 0.35 V vs. NHE. Combining with the Eg value of BMO-NS, the calculated VB potential of BMO-NS is 2.21 V vs. NHE. In addition, the specific surface areas of BMO-NS and BMO-bulk are 24.8 m^2/g and 6.1 m^2/g, respectively, which are revealed by nitrogen (N_2) adsorption-desorption isotherms (Fig. S5a). The monolayer BMO-NS with a bigger specific surface area would expose more surface unsaturated sites for absorbing related molecules. The photocurrent intensity test is conducted to investigate the photo-generated carrier separation and transfer ability of the prepared samples. As shown in Fig. S5b, the prepared BMO-NS exhibits a stronger photocurrent intensity than BMO-bulk, due to that the monolayer nanosheets structure of BMO-NS makes the photo-generated carries

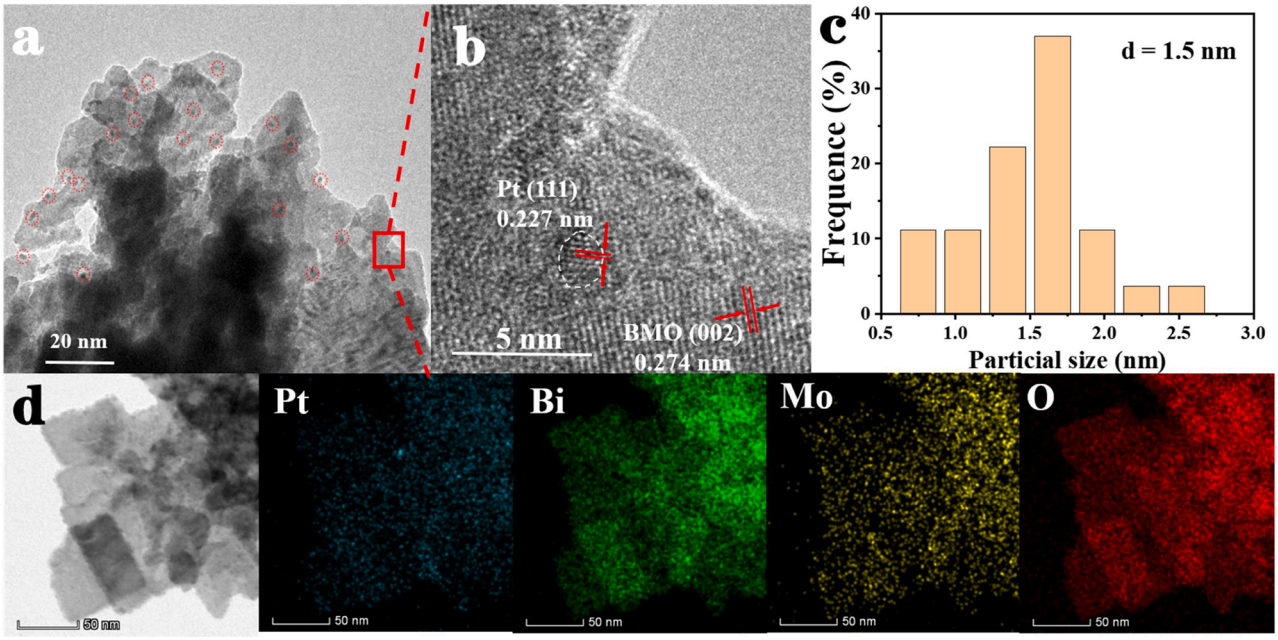

Fig. 2. TEM image (a); HRTEM image (b) of Pt/BMO-NS; size distribution of Pt (c) and element mapping images (d).

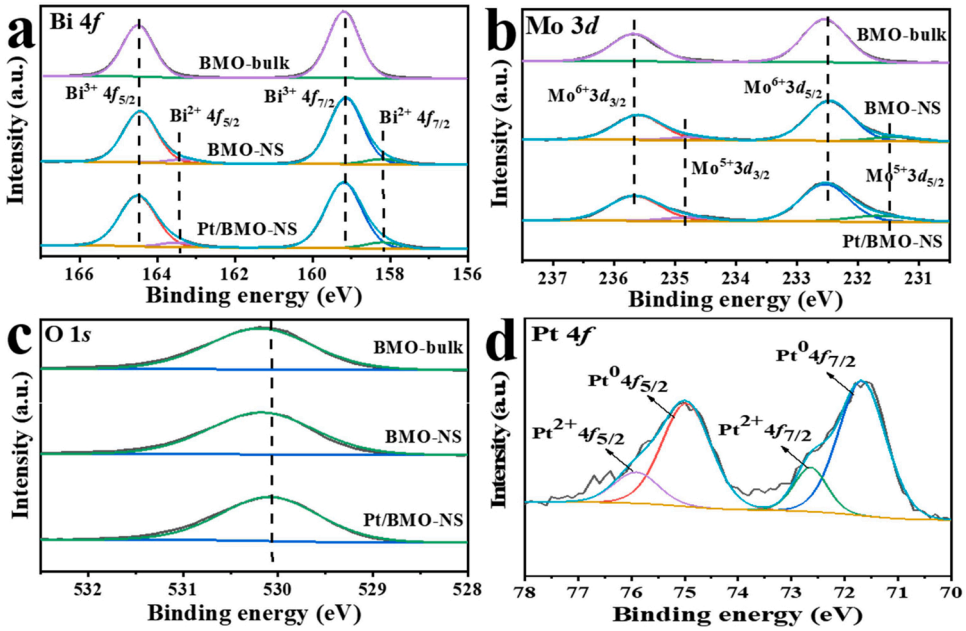

Fig. 3. XPS spectra of BMO-bulk, BMO-NS and Pt/BMO-NS, (a) Bi 4*f*, (b) Mo 3*d*, (c) O 1s and (d) Pt 4*f*.

transfer to the catalyst surface, easily. Pt/BMO-NS have the highest photocurrent intensity, indicating that the Pt clusters with high work function could serve as electron enrichment centers for transferring photo-generated electrons, greatly promoting the efficient separation of photo-generated electrons and holes. In addition, the electrochemical impedance spectroscopy results (Fig. S5c) also exhibit the excellent photo-generated carries separation and transfer ability of Pt/BMO-NS. All the results suggest that Pt/BMO-NS has good visible light absorption property, suitable VB and CB potentials, large specific surface area and good ability for the separation of photo-generated carriers.

3.2. Performances of the prepared samples

The prepared samples are used to selective reduce 4-nitrostyrene to 4-vinylaniline in the presence of ammonium formate under visible light irradiation. As shown in Table 1, it is observed that the pristine BMO-NS can directly reduce 4-nitrostyrene to 4-vinylaniline with the conversion of 16% which is 4 times higher than BMO-bulk. The better performance of BMO-NS is due to the monolayer nanosheets structure and rich surface unsaturated sites of BMO-NS. After loading Pt clusters, Pt/BMO-bulk and Pt/BMO-NS exhibit better performance for the reduction of 4-nitrostyrene to 4-vinylaniline, especially for Pt/BMO-NS, achieving the highest conversion of 4-nitrostyrene (≈100%) with high selectivity of 4-vinylaniline (≈100%) and a quantum yield (QY) of 1.7%. This may be benefit from the surface synergistic effect between monolayer BMO-NS and Pt clusters. In addition, the reduction of 4-nitrostyrene without $HCOONH_4$ is conducted as shown in Entry 5,6. BMO-NS and Pt/BMO-NS can convert little 4-nitrostyrene in methanol. However, the selectivity of 4-vinylaniline is only about 20% while the main product is 4-ethylaniline, suggesting that $HCOONH_4$ as hydrogen source is beneficial to the prioritized reduction of $-NO_2$ groups. In addition, the conversion of 4-nitrostyrene is greatly improved with $HCOONH_4$ (Entry 4) than that without $HCOONH_4$ (Entry 6), implying that the synergistic effect of Pt clusters and BMO-NS greatly promote the dissociation of $HCOONH_4$ to enhance the photocatalytic performance. The reduction of 4-nitrostyrene without light irradiation is also explored. It is clear that the 4-nitrostyrene cannot be reduced over BMO-NS without light irradiation, indicating the reduction of 4-nitrostyrene over BMO-NS is a

Table 1
Selective reduction of 4-nitrostyrene over the prepared samples.

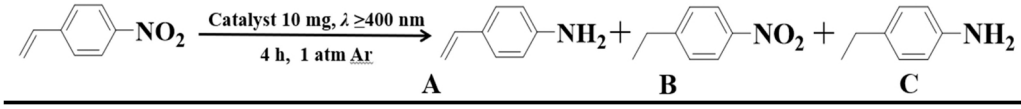

Entry	Catalysts	Solvent	hv	T (K)	Conv. (%)	Sel. (%)		
						A	B	C
1	BMO-bulk	$HCOONH_4$/methanol	+	305	4	98	–	2
2	BMO-NS	$HCOONH_4$/methanol	+	305	16	99	–	1
3	Pt/BMO-bulk	$HCOONH_4$/methanol	+	305	12	99	–	1
4	Pt/BMO-NS	$HCOONH_4$/methanol	+	305	≈ 100	≈ 100	–	–
5	BMO-NS	methanol	+	305	10	20	–	80
6	Pt/BMO-NS	methanol	+	305	22	22	–	78
7	BMO-NS	$HCOONH_4$/methanol	–	305	–	–	–	–
8	Pt/BMO-NS	$HCOONH_4$/methanol	–	305	11	99	–	1
9	Pt/BMO-NS	$HCOONH_4$/methanol	–	313	24	98	–	2
10	Pt/BMO-NS	$HCOONH_4$/methanol	–	333	38	95	–	5

Reaction condition: catalyst 10 mg, solvent 1.5 mL, 4-nitrostyrene 0.1 mmol, 1 atm Ar, $\lambda \geq 400$ nm, time 4 h.

photocatalytic process. However, 11% of the 4-nitrostyrene can be reduced to 4-vinylaniline over Pt/BMO-NS in the dark, indicating the reaction can be conducted in a thermal catalytic route after introducing Pt clusters. We further used oil bath heating to control the reaction temperature at 313 K and 333 K for studying the influence of thermal effect in the dark. It can be observed that the conversion of 4-nitrostyrene is improved with the increasing temperature, but the selectivity of 4-vinylaniline is decreased. It reveals that temperature can accelerate the reaction rate, but it cannot control the selectivity of 4-vinylaniline. The C═C groups would be more unstable at high temperatures. Considering a thermocouple during the photocatalytic experiments, the actual reaction temperature is measured to be 305 K. It is worth mentioning that even the temperatures are 313 K and 333 K, the dark conversions of 4-nitrostyrene are only 24% and 38%, respectively, which are far below the conversion at 305 K with visible light irradiation, suggesting that photocatalysis play a dominant role in this reaction.

To deeply study the selectivity reduction of 4-nitrostyrene to 4-vinylaniline over Pt/BMO-NS, a series of control experiments are further conducted. As shown in Fig. 4, the reduction of 4-nitrostyrene over Pt/BMO-NS with different reaction times is studied. It can be observed that the conversion of 4-nitrostyrene is gradually increased as time increases. When the reaction time is 4 h, 4-nitrostyrene can be completely converted to 4-vinylaniline. After 4 h, the 4-vinylaniline is further hydrogenated to 4-ethylaniline. These results indicate that the -NO_2 groups of 4-nitrostyrene could be preferentially absorbed and reduced over Pt/BMO-NS in the presence of $HCOONH_4$. Then, the free H species further achieves the hydrogenation of C═C groups of 4-vinylaniline, forming 4-ethylaniline. In addition, Table 1 shows that $HCOONH_4$ as hydrogen source is beneficial to the selective reduction 4-nitrostyrene to 4-vinylaniline. To reveal the optimal concentrations of $HCOONH_4$, the reduction of 4-nitrostyrene over Pt/BMO-NS with different concentrations of $HCOONH_4$ is conducted as shown in Fig. S6. The conversion of 4-nitrostyrene is improved as the concentrations of $HCOONH_4$ increase and the selectivity of 4-vinylaniline is kept above 98%. The best performance is obtained when the $HCOONH_4$ is saturated. We also investigate the performance of Pt/BMO-NS for the reduction of 4-nitrostyrene using difference hydrogen sources (Table S2). To avoid the influence of methanol as hydrogen, the toluene is used as the solvent. When the hydrogen source is $NaBH_4$, the conversion of 4-nitrostyrene without catalyst is 16% with a low selectivity of 11% for 4-vinylaniline. The conversion of 4-nitrostyrene can be improved to 40% using Pt/BMO-NS as the photocatalyst, and the selectivity of 4-vinylaniline is also increased to 36%. This result indicates that $NaBH_4$ as hydrogen source can uncontrollably reduce 4-nitrostyrene and Pt/BMO-NS with abundant surface sites can push the selective reduction of 4-nitrostyrene to 4-vinylaniline. Moreover, H_2 as hydrogen source is also showed a low selectivity of 4-vinylaniline. These results further confirm that $HCOONH_4$ as hydrogen source can help the selective reduction 4-nitrostyrene to 4-vinylaniline. The recycle experiment is also conducted to reveal the catalytic stability of Pt/BMO-NS (Fig. S7a). It is obvious that Pt/BMO-NS still keeps a high catalytic performance after 4 recycle and the XRD pattern of Pt/SWO-NS after 4 times recycle (Fig. S7b) is basically unchanged. In addition, TEM images and element mapping images of Pt/BMO-NS (Fig. S11) also exhibit the good dispersion of Pt element over BMO-NS after 4 times recycle, indicating its good structural stability. These results confirm that the prepared Pt/BMO-NS exhibits excellent stability.

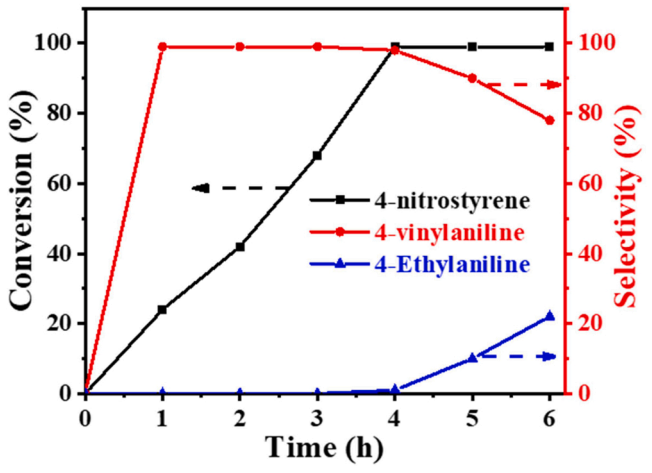

Fig. 4. The reduction of 4-nitrostyrene over Pt/BMO-NS with different reaction time.

The general applicability of prepared Pt/BMO-NS is explored via selectively reducing other nitroarenes with different reducible groups. As shown in Table 2, Pt/BMO-NS exhibits good performance for the selective reduction of halogenated nitrobenzene in only 2 h. The stronger electron-withdrawing ability of -Cl, -Br, -I groups, the better photocatalytic activities would be. This is because that -Cl, -Br, -I groups with strong electronegativity would make the electron density of -NO_2 groups decreased. Thus, the more electron-deficient -NO_2 group can be reduced easily. Quite the opposite, -C═C groups as electron-donating group would increase the electron density of -NO_2 groups, making it hard to be reduced. In addition, 4-nitrobenzaldehyde can be selectively reduced to 4-aminobenzaldehyde over Pt/BMO-NS with high conversion (98%) and high selectivity (99%). These results demonstrate that Pt/BMO-NS can preferentially reduce -NO_2 groups of nitroarenes rather than other reducible groups in the presence of $HCOONH_4$.

3.3. Photocatalytic mechanism

Based on the experiment results for the reduction of 4-nitrostyrene, it is not difficult to find that BMO-NS, Pt clusters and $HCOONH_4$ play important roles in photocatalytic performance. To reveal their respective roles for the reduction of 4-nitrostyrene, the absorption behavior of 4-nitrostyrene molecules over the catalyst and the main active species are further investigated. *In situ* FTIR spectra of BMO-NS absorbed 4-nitrostyrene (Fig. 5a) are used to reveal the absorption behavior of 4-nitrostyrene molecules on the monolayer BMO-NS surface. Several characteristic peaks assigned to 4-nitrostyrene (1597, 1515 and 1345 cm^{-1}) can be observed after adsorbing 4-nitrostyrene for 20 min at room temperature (Fig. 5a (2)). Even though after further degassing in vacuum to remove excess 4-nitrostyrene, these characteristic peaks still be existed (Fig. 5a (3)), revealing that there is a strong chemisorption interaction between BMO-NS and 4-nitrostyrene molecule. The characteristic peak at 1597 cm^{-1} is attributed to the stretching vibration of C═C ($\upsilon_{C=C}$) [47] while the characteristic peaks with a wavenumber of

Table 2
The photocatalytic reduction of different substrates over Pt/BMO-NS.

Entry	Substrates	Products	Time (h)	Conv. (%)	Sel. (%)
1	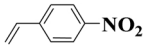	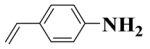	4	≈100%	≈100%
2	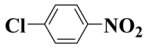	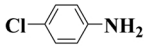	2	98	98
3	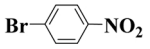	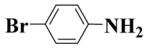	2	92	98
4	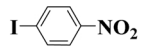	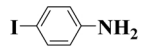	2	84	95
5	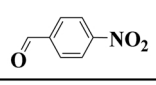	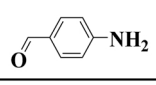	4	98	99

Reaction condition: catalyst 10 mg, 1.375 mmol/mL $HCOONH_4$/methanol solution 1.5 mL, 4-nitrostyrene 0.1 mmol, 1 atm Ar, $\lambda \geq 400$ nm, time 4 h.

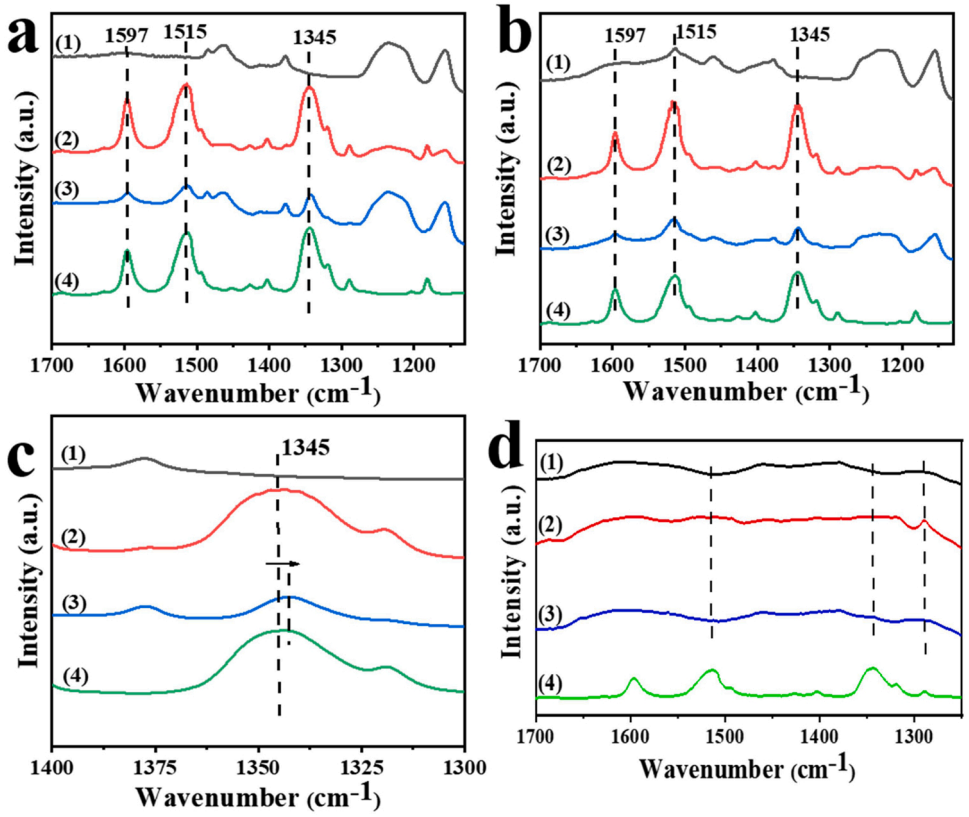

Fig. 5. In situ FTIR spectra of BMO-NS (a), Pt/BMO-NS (b) and BMO-bulk (d) absorbed 4-nitrostyrene. (c) Enlarged view of A. (1) After degassing in vacuum at 180 ℃ for 3 h, (2) adsorbing 4-nitrostyrene for 20 min at room temperature (physisorption + chemisorption), (3) further degassing in vacuum at 150 ℃ for 5 min (chemisorption), and (4) FTIR spectra of 4-nitrostyrene.

1515 and 1345 cm^{-1} are assigned to the stretching vibration of -NO_2 [40]. It is worth noting that after further degassing, the characteristic peak of the stretching vibration of -NO_2 at 1345 cm^{-1} shift to low wavenumber while the characteristic peak of C═C has no obvious shift, which can be clearly observed in Fig. 5c. This result indicates that the -NO_2 groups of 4-nitrostyrene can be selectively chemisorbed on BMO-NS via forming surface coordination species [35], promoting the reduction of 4-nitrostyrene towards 4-vinylaniline. In addition, in situ FTIR spectra of Pt/BMO-NS absorbed 4-nitrostyrene are provided to study the influence of Pt clusters for the adsorption of 4-nitrostyrene. As shown in Fig. 5b, the adsorption behavior of 4-nitrostyrene on Pt/BMO-NS is similar to that on BMO-NS, suggesting that few Pt clusters on BMO-NS have a very negligible influence for absorbing 4-nitrostyrene molecules. The in situ FTIR spectra of BMO-bulk absorbed 4-nitrostyrene are also conducted. Fig. 5d shows a weak absorption of 4-nitrostyrene over BMO-bulk. This is the reason for the low photocatalytic performance of BMO-bulk. It also further indicates that BMO-NS with rich surface sites is beneficial to selectively chemisorb 4-nitrostyrene molecules.

What sites on monolayer BMO-NS are responsible for absorbing -NO_2 groups in 4-nitrostyrene? As mentioned before, the -NO_2 as electron-deficient group trends to be absorbed on the nucleophilic sites such as surface Lewis base sites. Thus, CO_2-TPD experiments are used to determine the surface basicity of BMO-NS and BMO-bulk. As shown in Fig. S8, the BMO-NS sample has an obvious peak of the absorption for CO_2 molecules, but there is almost no peak for absorption of CO_2 molecules on BMO-bulk. This result demonstrates that monolayer BMO-NS have rich surface Lewis base sites while the surface base sites of BMO-bulk are poor [50]. These Lewis base sites may be derived from the surface unsaturated Bi^{2+} or Mo^{5+} atoms of monolayer BMO-NS. The Bi^{2+} and Mo^{5+} with a higher electron cloud density are good electron donors which can combine with electron-deficient -NO_2 groups easily via surface coordination. The possible adsorption behavior of 4-nitrostyrene molecules over monolayer BMO-NS is shown in Fig. S9. It can be observed that 4-nitrostyrene molecules would be chemisorbed on BMO-NS via a Bi···O-N or Mo···O-N coordination, forming surface coordination species. It would cause the effective activation of 4-nitrostyrene molecules and the further photocatalytic reduction of the activated 4-nitrostyrene molecules can be more easily.

Additionally, XPS spectra of Pt/BMO-NS before and after absorbing 4-nitrostyrene further investigate the binding energy change of Bi, Mo, O, Pt elements. As shown in Fig. 6b, after absorbing 4-nitrostyrene, O1s shows a new peak at binding energy 532.1 eV which is assigned to absorbed -NO_2 groups, confirming the strong chemisorption between BMO-NS and 4-nitrostyrene molecules. Moreover, it is obvious that the peaks of Bi^{2+} at binding energy 158.2 eV and 163.4 eV are almost disappeared and the binding energy of Bi 4 f shifts to high binding energy after the adsorption of 4-nitrostyrene (Fig. 6a), suggesting that the electron cloud density of Bi is decreased. It confirms the formation of Bi···O-N coordination between the 4-nitrostyrene molecules and Bi^{2+} sites of BMO-NS, resulting in the electrons transfer from Bi^{2+} to the -NO_2 groups via the Bi···O-N coordination. Meanwhile, the binding energy change of Mo 3d after absorbing 4-nitrostyrene is similar to that of Bi 4 f. The ratio of Mo^{5+} is decreased after absorbing 4-nitrostyrene (Table S3). These results confirm that surface Bi^{2+} and Mo^{5+} would combine with -NO_2 groups via a Bi···O-N and Mo···O-N coordination. However, the binding energy of Pt is hardly changed, also indicating that Pt clusters have a negligible influence for absorbing 4-nitrostyrene molecules. It further confirms that the rich surface Bi^{2+} and Mo^{5+} sites in BMO-NS as Lewis acid sites provide enormous contribution to selectively chemisorb and activate -NO_2 groups, greatly improving the selectivity of 4-vinylaniline. In addition, UV–vis DRS spectra of BMO-NS and BMO-bulk adsorbed 4-nitrostyrene are shown in Fig. S10. The UV–vis DRS spectra of BMO-NS and BMO-bulk both have red shift after absorbing 4-

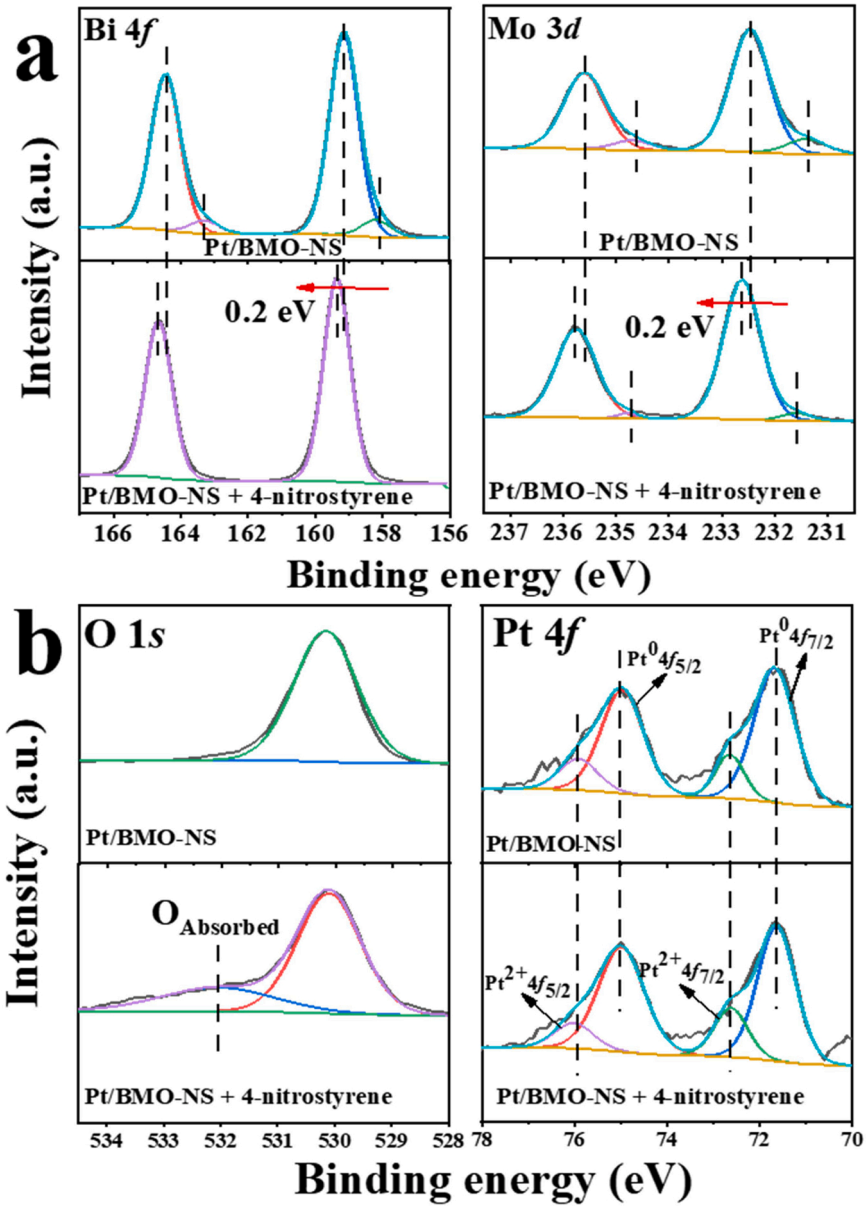

Fig. 6. XPS spectra of Pt/BMO-NS and Pt/BMO-NS absorbed 4-nitrostyrene, (a) Bi 4 *f* and Mo 3*d*; (b) O 1 *s* and Pt 4 *f*.

nitrostyrene molecule, also indicating that the formation of surface coordination species between the prepared samples and 4-nitrostyrene molecules [35]. Furthermore, BMO-NS exhibits a stronger red shift than BMO-bulk. This is benefited from the rich surface Bi^{2+} and Mo^{5+} sites of monolayer BMO-NS. All the above results successfully reveal the surface/interface interaction between the 4-nitrostyrene molecules and the surface active sites of monolayer BMO-NS at a molecule level.

The selective absorption and activation of $-NO_2$ groups is the precondition for the precise synthesis of 4-vinylaniline. Moreover, the further conversion of activated 4-nitrostyrene by active species is the rate-determining step for the selective reduction of 4-nitrostyrene to 4-vinylaniline. It is well known that $HCOONH_4$ can be dissociated to $\cdot CO_2^-$ and H^+. $\cdot CO_2^-$ radicals have strong reducibility (E_0 ($CO_2/\cdot CO_2^-$) $= -1.8$ V) which prefer to reduce electron-deficient $-NO_2$ groups [51]. To further confirm the formation of the $\cdot CO_2^-$ active species, the EPR test for Pt/BMO-NS, BMO-NS and BMO-Bulk is conducted in a 1.375 mmol/mL $HCOONH_4$/methanol solution with DMPO at Ar atmosphere. For the EPR spectra of BMO-NS and BMO-Bulk (Fig. 7a), no EPR signal can be observed in the dark but the characteristic peaks with a sextet of DMPO-$\cdot CO_2^-$ are exhibited under visible light irradiation [38]. This result indicates that the dissociation of $HCOONH_4$ to $\cdot CO_2^-$ can be proceed over Bi_2MoO_6 by a photocatalytic process. Some studies have reported that photo-generated holes can react with $HCOO^-$ to produce $\cdot CO_2^-$ and H^+ [23]. Therefore, the photo-generated holes of Bi_2MoO_6 with a more positive VB position (2.21 V vs. NHE) would directly dissociate $HCOO^-$ to $\cdot CO_2^-$ and H^+ for reducing 4-nitrostyrene to 4-vinylaniline. After loading Pt clusters, the characteristic peaks of $\cdot CO_2^-$ can be clearly observed in the dark, indicating that Pt clusters possess the ability of decomposing $HCOONH_4$ to $\cdot CO_2^-$ for the reduction of 4-nitrostyrene. Moreover, a stronger characteristic peak of $\cdot CO_2^-$ is observed under visible light. It may be because that photo-generated electrons of BMO-NS could promote Pt clusters to decompose $HCOO^-$ while photo-generated holes of BMO-NS would also react with $HCOO^-$ to produce $\cdot CO_2^-$. To further prove the presence of active ·H species, the EPR test using N-tert-Butyl-α-phenylnitrone (PBN) as a radical trap at the Ar atmosphere is conducted. As shown in Fig. 7(b), a sextet characteristic peak which is attributed to the carbon-centered radical [52], i.e. PBN-$\cdot CO_2^-$ is observed. It is consistent with the results of Fig. 7(a). In

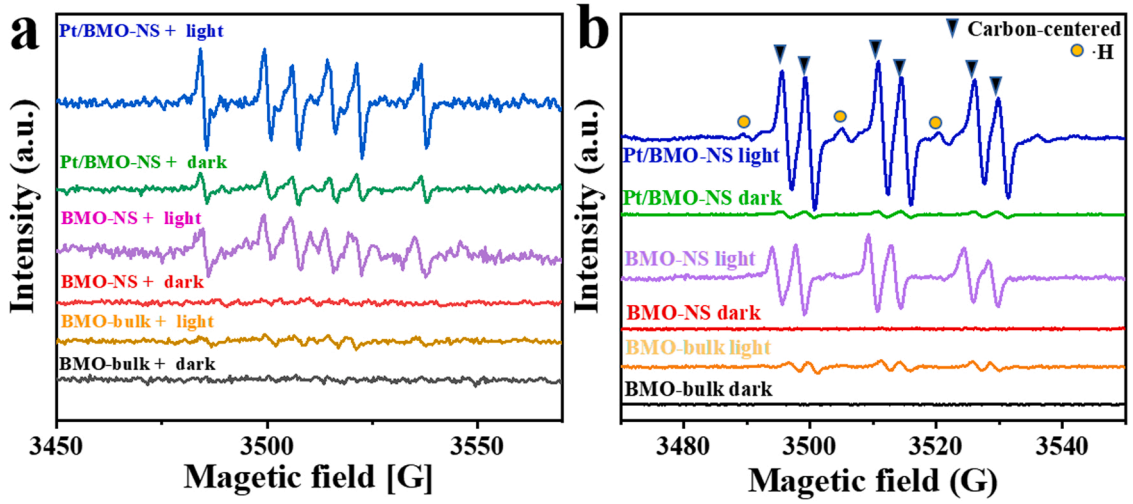

Fig. 7. EPR spectra of Pt/BMO-NS, BMO-NS and BMO-Bulk in a 1.375 mmol/mL $HCOONH_4$/methanol solution with DMPO (a); PBN (b).

addition, some new characteristic peaks attributed to ·H [47] are observed in the EPR spectrum of Pt/BMO-NS under visible light irradiation. This result confirms the formation of ·H. However, there is no signal of ·H in the EPR spectra of BMO-NS and BMO-bulk. The reason is that the photogenerated hole would dissociate $HCOO^-$ to H^+ rather than ·H. It also indicates that Pt clusters as functional sites would gather photogenerated electrons to convert H^+ to ·H. The synergistic effect between Pt clusters and BMO-NS would greatly accelerate the dissociation of $HCOO^-$ to produce abundant $\cdot CO_2^-$ and active ·H. These active species would further attack the activated 4-nitrostyrene molecule on BMO-NS, achieving the efficient reduction of 4-nitrostyrene to 4-vinylaniline.

The possible processes for the dissociation of $HCOONH_4$ and the reduction of $-NO_2$ groups over Pt/BMO-NS are proposed as shown in Eqs. (1–7). $HCOONH_4$ would be dissolved to produce $HCOO^-$ and NH_4^+ in methanol solution (Eq. (1)). Then, Pt clusters would react with $HCOO^-$ to form little $\cdot CO_2^-$ and Pt-H (Eq. (2)). BMO-NS can be photoexcited to produce photo-generated electrons (e^-) and holes (h^+) (Eq. (3)). photo-generated holes (h^+) would react with $HCOO^-$ to produce $\cdot CO_2^-$ and H^+ (Eq. (4)). The photo-generated electron would transfer to Pt clusters for further promoting the formation of active ·H species (Eqs. (5, 6)), driving the reaction (Eq. (2)) to produce more $\cdot CO_2^-$. Finally, the $\cdot CO_2^-$ and ·H as active species would react with $-NO_2$, achieving the reduction of 4-nitrostyrene to 4-vinylaniline (Eq. (7)).

$$HCOONH_4 \rightarrow HCOO^- + NH_4^+ \quad (1)$$

$$Pt + HCOO^- \rightarrow \cdot CO_2^- + Pt\text{-}H \quad (2)$$

$$BMO\text{-}NS + h\nu \rightarrow e^- + h^+ \quad (3)$$

$$h^+ + HCOO^- \rightarrow H^+ + \cdot CO_2^- \quad (4)$$

$$H^+ + e^- \rightarrow \cdot H \quad (5)$$

$$Pt\text{-}H + e^- \rightarrow Pt + \cdot H \quad (6)$$

$$6 \cdot CO_2^- + 6 \cdot H + -NO_2 \rightarrow 6CO_2 + -NH_2 + 2\,H_2O \quad (7)$$

Combining with the above experiments results, a possible catalytic mechanism for the selective reduction of 4-nitrostyrene to 4-vinylaniline

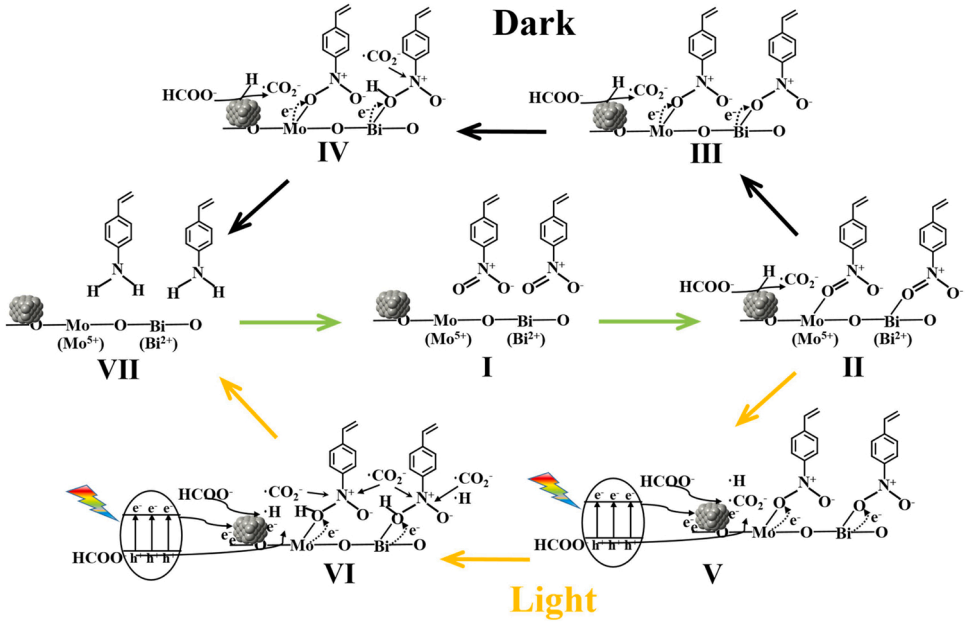

Scheme 1. Possible mechanism for the selective reduction of 4-nitrostyrene to 4-vinylaniline over Pt/BMO-NS.

over Pt/BMO-NS is proposed to deeply elucidate the surface/interface transformation process. As shown in Scheme 1, firstly, the electron-deficient -NO_2 groups of 4-nitrostyrene molecules could be selectively chemisorbed on the surface Bi^{2+} and Mo^{5+} sites of BMO-NS via the Bi···O-N and Mo···O-N coordination while Pt clusters would react with $HCOO^-$ to form little $\cdot CO_2^-$ and Pt-H in the dark(**II**). Then the reduction of 4-nitrostyrene would be conducted in two routes. In the dark, the Bi···O-N and Mo···O-N coordination make the interface charges transfer from Bi and Mo to the -NO_2 groups, causing the activation of -NO_2 groups (**III**). The little $\cdot CO_2^-$ and ·H further reduce the -NO_2 groups (**IV**), resulting in that 11% of the 4-nitrostyrene being converted to 4-vinylaniline. Meanwhile, under the visible light irradiation, the multiple synergistic effects of the Pt clusters, photogenerated electrons and holes cause the efficient dissociation of $HCOONH_4$ to $\cdot CO_2^-$ and active ·H species and the -NO_2 groups are activated via the Bi···O-N and Mo···O-N coordination (**V**). The rich $\cdot CO_2^-$ and active ·H species would attack the activated -NO_2 groups (**VI**), achieving the efficient conversion of 4-nitrostyrene to 4-vinylaniline. 4-vinylaniline has the nature of electron donor and is not easily absorbed at the Bi^{2+} and Mo^{5+} sites. Thus, the formed 4-vinylaniline would be desorbed over the surface of Pt/BMO-NS while the Bi^{2+} and Mo^{5+} sites are recovered for the next cycle (**VII**).

4. Conclusion

In summary, the composite photocatalyst of monolayer BMO-NS nanosheet with Pt clusters is successfully designed and prepared for the selective reduction of 4-nitrostyrene to 4-vinylaniline in the presence of $HCOONH_4$, exhibiting the efficient conversion of 4-nitrostyrene (≈100%) with high selectivity for 4-vinylaniline (≈100%). Compared with BMO-bulk, monolayer BMO-NS nanosheet exposes more surface unsaturated Bi^{2+} and Mo^{5+} sites to serve as Lewis base sites which greatly promote the selective absorption and activation of 4-nitrostyrene molecules via the Bi···O-N or Mo···O-N coordination. The multiple synergistic effects of the Pt clusters, photogenerated electrons and holes cause the efficient dissociation of $HCOONH_4$ to $\cdot CO_2^-$ and active ·H species, greatly supporting the reduction of 4-nitrostyrene to 4-vinylaniline. Finally, a possible catalytic process is proposed to elucidate the surface/interface interaction and transformation of the 4-nitrostyrene molecules over Pt/ BMO-NS. This work successfully provides a photocatalytic route to achieve the selective reduction of 4-nitrostyrene to 4-vinylaniline in a mild condition via photocatalytic hydrogen transfer and gives an in-depth view to understand the selective absorption, activation and photocatalytic transformation of organic molecules over the surface of metal/monolayer nanosheets.

CRediT authorship contribution statement

Yingzhang Shi: Conceptualization, Investigation, Writing – original draft, Formal analysis. **Zhiwen Wang:** Validation, Formal analysis. **Cheng Liu:** Formal analysis. **Taikang Wu:** Data curation. **Rui Liu:** Validation. **Ling Wu:** Conceptualization, Writing – review & editing.

Declaration of Competing Interest

The authors declare that they have no known competing financial interests or personal relationships that could have appeared to influence the work reported in this paper.

The authors declare no competing financial interest.

Acknowledgments

This work was supported by the National Natural Science Foundation of China (21872032).

Appendix A. Supporting information

Supplementary data associated with this article can be found in the online version at doi:10.1016/j.apcatb.2021.121010.

References

[1] R.S. Downing, P.J. Kunkeler, H. Van Bekkum, Catalytic syntheses of aromatic amines, Catal. Today 37 (1997) 121–136, https://doi.org/10.1016/S0920-5861(97)00005-9.
[2] A.M. Tafesh, J. Weiguny, A review of the selective catalytic reduction of aromatic nitro compounds into aromatic amines, isocyanates, carbamates, and ureas using CO, Chem. Rev. 96 (1996) 2035–2052, https://doi.org/10.1021/cr950083f.
[3] S. Zhang, C.R. Chang, Z.Q. Huang, J. Li, Z. Wu, Y. Ma, Z. Zhang, Y. Wang, Y. Qu, High catalytic activity and chemoselectivity of sub-nanometric Pd clusters on porous nanorods of CeO_2 for hydrogenation of nitroarenes, J. Am. Chem. Soc. 138 (2016) 2629–2637, https://doi.org/10.1021/jacs.5b11413.
[4] A. Corma, P. Serna, Chemoselective hydrogenation of nitro compounds with supported gold catalysts, Science 313 (2006) 332–334, https://doi.org/10.1126/science.1128383.
[5] H. Wei, X. Liu, A. Wang, L. Zhang, B. Qiao, X. Yang, Y. Huang, S. Miao, J. Liu, T. Zhang, FeOx-supported platinum single-atom and pseudo-single-atom catalysts for chemoselective hydrogenation of functionalized nitroarenes, Nat. Commun. 5 (2014) 1–8, https://doi.org/10.1038/ncomms6634.
[6] L. Zhang, M. Zhou, A. Wang, T. Zhang, Selective hydrogenation over supported metal catalysts: from nanoparticles to single atoms, Chem. Rev. 120 (2020) 683–733, https://doi.org/10.1021/acs.chemrev.9b00230.
[7] J. Li, Y. Long, Y. Liu, L. Zhang, Q. Wang, X. Wang, S. Song, H. Zhang, Robust synthesis of gold-based multishell structures as plasmonic catalysts for selective hydrogenation of 4-nitrostyrene, Angew. Chem. Int. Ed. 59 (2020) 1103–1107, https://doi.org/10.1002/anie.201910836.
[8] J. Mao, W. Chen, W. Sun, Z. Chen, J. Pei, D. He, C. Lv, D. Wang, Y. Li, Rational control of the selectivity of a ruthenium catalyst for hydrogenation of 4-nitrostyrene by strain regulation, Angew. Chem. Int. Ed. 56 (2017) 11971–11975, https://doi.org/10.1002/anie.201706645.
[9] M.J. Beier, J.M. Andanson, A. Baiker, Tuning the chemoselective hydrogenation of nitrostyrenes catalyzed by ionic liquid-supported platinum nanoparticles, ACS Catal. 2 (2012) 2587–2595, https://doi.org/10.1021/cs300529y.
[10] N. Yang, H. Cheng, X. Liu, Q. Yun, Y. Chen, B. Li, B. Chen, Z. Zhang, X. Chen, Q. Lu, J. Huang, Y. Huang, Y. Zong, Y. Yang, L. Gu, H. Zhang, Amorphous/crystalline hetero-phase Pd nanosheets: one-pot synthesis and highly selective hydrogenation reaction, Adv. Mater. 30 (2018) 1–5, https://doi.org/10.1002/adma.201803234.
[11] H. Yamashita, K. Mori, Y. Kuwahara, T. Kamegawa, M. Wen, P. Verma, M. Che, Single-site and nano-confined photocatalysts designed in porous materials for environmental uses and solar fuels, Chem. Soc. Rev. 47 (2018) 8072–8096, https://doi.org/10.1039/c8cs00341f.
[12] W. Wang, T. An, G. Li, D. Xia, H. Zhao, J.C. Yu, P.K. Wong, Earth-abundant Ni_2P/g-C_3N_4 lamellar nanohydrids for enhanced photocatalytic hydrogen evolution and bacterial inactivation under visible light irradiation, Appl. Catal. B Environ. 217 (2017) 570–580, https://doi.org/10.1016/j.apcatb.2017.06.027.
[13] J. Xu, Z. Wang, Y. Zhu, Enhanced visible-light-driven photocatalytic disinfection performance and organic pollutant degradation activity of porous g-C_3N_4 nanosheets, ACS Appl. Mater. Interfaces 9 (2017) 27727–27735, https://doi.org/10.1021/acsami.7b07657.
[14] X. Lang, X. Chen, J. Zhao, Heterogeneous visible light photocatalysis for selective organic transformations, Chem. Soc. Rev. 43 (2014) 473–486, https://doi.org/10.1039/c3cs60188a.
[15] C. Gao, J. Wang, H. Xu, Y. Xiong, Coordination chemistry in the design of heterogeneous photocatalysts, Chem. Soc. Rev. 46 (2017) 2799–2823, https://doi.org/10.1039/c6cs00727a.
[16] J. Zhong, C. Wu, Q. Meng, X. Gao, T. Lei, C. Tung, L. Wu, A cascade cross-coupling and in situ hydrogenation reaction by visible light catalysis, Adv. Synth. Catal. 356 (2014) 2846–2852, https://doi.org/10.1002/adsc.201400588.
[17] M.M. Trandafir, F. Neaţu, I.M. Chirica, Ş. Neaţu, A.C. Kuncser, E.I. Cucolea, V. Natu, M.W. Barsoum, M. Florea, Highly efficient ultralow Pd loading supported on MAX phases for chemoselective hydrogenation, ACS Catal. 10 (2020) 5899–5908, https://doi.org/10.1021/acscatal.0c00082.
[18] B. Tamami, H. Mahdavi, Quaternized amino functionalized cross-linked polyacrylamide as a new solid-Liquid phase transfer catalyst in reduction of carbonyl compounds with $NaBH_4$, Tetrahedron 59 (2003) 821–826, https://doi.org/10.1016/S0040-4020(02)01588-0.
[19] M.M. Mohamed, M.S. Al-Sharif, Visible light assisted reduction of 4-nitrophenol to 4-aminophenol on Ag/TiO_2 photocatalysts synthesized by hybrid templates, Appl. Catal. B Environ. 142–143 (2013) 432–441, https://doi.org/10.1016/j.apcatb.2013.05.058.
[20] Y. Ma, Z. Li, Coupling plasmonic noble metal with TiO_2 for efficient photocatalytic transfer hydrogenation: M/TiO_2 (M = Au and Pt) for chemoselective transformation of cinnamaldehyde to cinnamyl alcohol under visible and 365 nm UV light, Appl. Surf. Sci. 452 (2018) 279–285, https://doi.org/10.1016/j.apsusc.2018.04.244.
[21] W. Wu, L. Wen, L. Shen, R. Liang, R. Yuan, L. Wu, A new insight into the photocatalytic reduction of 4-nitroaniline to p-phenylenediamine in the presence of alcohols, Appl. Catal. B Environ. 130–131 (2013) 163–167, https://doi.org/10.1016/j.apcatb.2012.10.025.

[22] R.A. Al-Alawi, K. Laxman, S. Dastgir, J. Dutta, Role of bonding mechanisms during transfer hydrogenation reaction on heterogeneous catalysts of platinum nanoparticles supported on zinc oxide nanorods, Appl. Surf. Sci. 377 (2016) 200–206, https://doi.org/10.1016/j.apsusc.2016.03.155.
[23] K. Doudrick, T. Yang, K. Hristovski, P. Westerhoff, Photocatalytic nitrate reduction in water: Managing the hole scavenger and reaction by-product selectivity, Appl. Catal. B Environ. 136–137 (2013) 40–47, https://doi.org/10.1016/j.apcatb.2013.01.042.
[24] Y. Wang, R. Qin, Y. Wang, J. Ren, W. Zhou, L. Li, J. Ming, W. Zhang, G. Fu, N. Zheng, Chemoselective hydrogenation of nitroaromatics at the nanoscale iron (III)–OH–platinum interface, Angew. Chem. Int. Ed. 59 (2020) 12736–12740, https://doi.org/10.1002/anie.202003651.
[25] K. Jing, J. Xiong, N. Qin, Y. Song, L. Li, Y. Yu, S. Liang, L. Wu, Development and photocatalytic mechanism of monolayer Bi_2MoO_6 nanosheets for the selective oxidation of benzylic alcohols, Chem. Commun. 53 (2017) 8604–8607, https://doi.org/10.1039/c7cc04052k.
[26] X. Xu, X. Ding, X. Yang, P. Wang, S. Li, Z. Lu, H. Chen, Oxygen vacancy boosted photocatalytic decomposition of ciprofloxacin over Bi_2MoO_6: Oxygen vacancy engineering, biotoxicity evaluation and mechanism study, J. Hazard. Mater. 364 (2019) 691–699, https://doi.org/10.1016/j.jhazmat.2018.10.063.
[27] X. Yang, S. Wang, N. Yang, W. Zhou, P. Wang, K. Jiang, S. Li, H. Song, X. Ding, H. Chen, J. Ye, Oxygen vacancies induced special CO_2 adsorption modes on Bi_2MoO_6 for highly selective conversion to CH_4, Appl. Catal. B Environ. 259 (2019), 118088, https://doi.org/10.1016/j.apcatb.2019.118088.
[28] Y. Chen, W. Yang, S. Gao, C. Sun, Q. Li, Synthesis of Bi_2MoO_6 nanosheets with rich oxygen vacancies by postsynthesis etching treatment for enhanced photocatalytic performance, ACS Appl. Nano Mater. 1 (2018) 3565–3578, https://doi.org/10.1021/acsanm.8b00719.
[29] Y. Xie, X. Shang, D. Liu, H. Zhao, Y. Gu, Z. Zhang, X. Wang, Non-noble metal thickness-tunable Bi_2MoO_6 nanosheets for highly efficient visible-light-driven nitrobenzene reduction into aniline, Appl. Catal. B Environ. 259 (2019), 118087, https://doi.org/10.1016/j.apcatb.2019.118087.
[30] J. Xiong, J. Di, H. Li, Atomically thin 2D multinary nanosheets for energy-related photo, electrocatalysis, Adv. Sci. 5 (2018), 1800244, https://doi.org/10.1002/advs.201800244.
[31] B. Luo, G. Liu, L. Wang, Recent advances in 2D materials for photocatalysis, Nanoscale 8 (2016) 6904–6920, https://doi.org/10.1039/c6nr00546b.
[32] H. Wang, X. Zhang, Y. Xie, Recent progress in ultrathin two-dimensional semiconductors for photocatalysis, Mater. Sci. Eng. R. Rep. 130 (2018) 1–39, https://doi.org/10.1016/j.mser.2018.04.002.
[33] F. Yi, H. Ren, J. Shan, X. Sun, D. Wei, Z. Liu, Wearable energy sources based on 2D materials, Chem. Soc. Rev. 47 (2018) 3152–3188, https://doi.org/10.1039/c7cs00849j.
[34] C. Tan, X. Cao, X.J. Wu, Q. He, J. Yang, X. Zhang, J. Chen, W. Zhao, S. Han, G. H. Nam, M. Sindoro, H. Zhang, Recent advances in ultrathin two-dimensional nanomaterials, Chem. Rev. 117 (2017) 6225–6331, https://doi.org/10.1021/acs.chemrev.6b00558.
[35] S. Liang, L. Wen, S. Lin, J. Bi, P. Feng, X. Fu, L. Wu, Monolayer HNb_3O_8 for selective photocatalytic oxidation of benzylic alcohols with visible light response, Angew. Chem. Int. Ed. 53 (2014) 2951–2955, https://doi.org/10.1002/anie.201311280.
[36] K. Jing, W. Ma, Y. Ren, J. Xiong, B. Guo, Y. Song, S. Liang, L. Wu, Hierarchical Bi_2MoO_6 spheres in situ assembled by monolayer nanosheets toward photocatalytic selective oxidation of benzyl alcohol, Appl. Catal. B Environ. 243 (2019) 10–18, https://doi.org/10.1016/j.apcatb.2018.10.027.
[37] J. Zou, Z. Wang, W. Guo, B. Guo, Y. Yu, L. Wu, Photocatalytic selective oxidation of benzyl alcohol over ZnTi-LDH: The effect of surface OH groups, Appl. Catal. B Environ. 260 (2020), 118185, https://doi.org/10.1016/j.apcatb.2019.118185.
[38] Y. Song, H. Wang, Z. Wang, B. Guo, K. Jing, Y. Li, L. Wu, Selective photocatalytic synthesis of haloanilines from halonitrobenzenes over multifunctional AuPt/monolayer titanate nanosheet, ACS Catal. 8 (2018) 9656–9664, https://doi.org/10.1021/acscatal.8b02662.
[39] C. Hu, R. Chen, N. Zheng, Chemical insights into interfacial effects in inorganic nanomaterials, Adv. Mater. 2006159 (2021) 1–10, https://doi.org/10.1002/adma.202006159.
[40] Y. Shi, H. Wang, Z. Wang, T. Wu, Y. Song, B. Guo, L. Wu, Pt decorated hierarchical Sb_2WO_6 microspheres as a surface functionalized photocatalyst for the visible-light-driven reduction of nitrobenzene to aniline, J. Mater. Chem. A. 8 (2020) 18755–18766, https://doi.org/10.1039/d0ta06099b.
[41] J. Liu, L. Cao, W. Huang, Z. Li, Preparation of AuPt alloy foam films and their superior electrocatalytic activity for the oxidation of formic acid, ACS Appl. Mater. Interfaces 3 (2011) 3552–3558, https://doi.org/10.1021/am200782x.
[42] Y. Zhang, Y. Shi, R. Chen, L. Tao, C. Xie, D. Liu, D. Yan, S. Wang, Enriched nucleation sites for Pt deposition on ultrathin WO_3 nanosheets with unique interactions for methanol oxidation, J. Mater. Chem. A. 6 (2018) 23028–23033, https://doi.org/10.1039/c8ta08636b.
[43] J. Divya, N.J. Shivaramu, E. Coetsee, R.E. Kroon, W. Purcell, H.C. Swart, Enhanced luminescence and photocatalytic activity of Bi_2O_3:Ho^{3+} needles, J. Alloy. Compd. 842 (2020), 155641, https://doi.org/10.1016/j.jallcom.2020.155641.
[44] J. Fu, J. Dong, R. Si, K. Sun, J. Zhang, M. Li, N. Yu, B. Zhang, M.G. Humphrey, Q. Fu, J. Huang, Synergistic effects for enhanced catalysis in a dual single-atom catalyst, ACS Catal. 11 (2021) 1952–1961, https://doi.org/10.1021/acscatal.0c05599.
[45] R. Wang, Y. Liu, G. Li, A. Wang, X. Wang, Y. Cong, T. Zhang, N. Li, Direct synthesis of methylcyclopentadiene with 2,5-hexanedione over zinc molybdates, ACS Catal. 11 (2021) 4810–4820, https://doi.org/10.1021/acscatal.1c00223.
[46] Y. Zheng, T. Zhou, X. Zhao, W.K. Pang, H. Gao, S. Li, Z. Zhou, H. Liu, Z. Guo, Atomic interface engineering and electric-field effect in ultrathin Bi_2MoO_6 nanosheets for superior lithium ion storage, Adv. Mater. 29 (2017) 1–8, https://doi.org/10.1002/adma.201700396.
[47] H. Wang, Y. Shi, Z. Wang, Y. Song, M. Shen, B. Guo, L. Wu, Selective hydrogenation of cinnamaldehyde to hydrocinnamaldehyde over Au-Pd/ultrathin $SnNb_2O_6$ nanosheets under visible light, J. Catal. 396 (2021) 374–386, https://doi.org/10.1016/j.jcat.2021.03.011.
[48] Y. Ma, B. Chi, W. Liu, L. Cao, Y. Lin, X. Zhang, X. Ye, S. Wei, J. Lu, Tailoring of the proximity of platinum single atoms on CeO_2 using phosphorus boosts the hydrogenation activity, ACS Catal. 9 (2019) 8404–8412, https://doi.org/10.1021/acscatal.9b01536.
[49] S. Cao, B. Shen, T. Tong, J. Fu, J. Yu, 2D/2D Heterojunction of ultrathin MXene/Bi_2WO_6 nanosheets for improved photocatalytic CO_2 reduction, Adv. Funct. Mater. 28 (2018) 1–11, https://doi.org/10.1002/adfm.201800136.
[50] L. Zhu, X.Q. Liu, H.L. Jiang, L.B. Sun, Metal-organic frameworks for heterogeneous basic catalysis, Chem. Rev. 117 (2017) 8129–8176, https://doi.org/10.1021/acs.chemrev.7b00091.
[51] W. Wu, G. Liu, Q. Xie, S. Liang, H. Zheng, R. Yuan, W. Su, L. Wu, A simple and highly efficient route for the preparation of p-phenylenediamine by reducing 4-nitroaniline over commercial CdS visible light-driven photocatalyst in water, Green. Chem. 14 (2012) 1705–1709, https://doi.org/10.1039/c2gc35231a.
[52] X. Cao, Z. Chen, R. Lin, W.C. Cheong, S. Liu, J. Zhang, Q. Peng, C. Chen, T. Han, X. Tong, Y. Wang, R. Shen, W. Zhu, D. Wang, Y. Li, A photochromic composite with enhanced carrier separation for the photocatalytic activation of benzylic C–H bonds in toluene, Nat. Catal. 1 (2018) 704–710, https://doi.org/10.1038/s41929-018-0128-z.